Soliton rains in a fiber laser: An experimental study

Souad Chouli and Philippe Grelu
Laboratoire Interdisciplinaire Carnot de Bourgogne, UMR 5209 CNRS, Université de Bourgogne, 9 avenue A. Savary, Boîte Postale 47870, 21078 Dijon Cedex, France
(Received 30 April 2010; published 28 June 2010)

Rains of solitons constitute a class of nonlinear dynamics of dissipative soliton ensembles that we briefly reported in Opt. Express **17**, 11776 (2009) from a fiber laser experiment. The existence of a relatively intense noisy background together with several tens of soliton pulses aggregated in a condensed soliton phase constitutes a necessary condition for their appearance. New soliton pulses form spontaneously from the background fluctuations and drift until they reach the condensed soliton phase. We here relate in detail the experimental conditions under which soliton rains manifest and their key features, describe related dynamics observed in their vicinity, and propose an explanation for soliton rain dynamics.

DOI: 10.1103/PhysRevA.81.063829 PACS number(s): 42.65.Tg, 05.45.Yv, 42.60.Fc, 42.81.Dp

I. INTRODUCTION

Passively mode-locked fiber lasers represent a mature technology that led to the manufacturing of compact, robust, and versatile short and ultrashort pulsed sources for numerous market applications. They also constitute an ideal platform for the exploration of new areas of nonlinear dynamics in an open, dissipative environment, since under moderate pumping power significant interplays between various physical effects can be experienced [1]. These effects include dispersive effects such as Kerr nonlinearity and chromatic dispersion, and, according to the cavity design, can comprise linear and nonlinear birefringence. Dissipative effects such as linear and saturable losses, as well as bandwidth-limited gain, are also likely to have a dominant impact on the resulting dynamics. Several contemporary nonlinear dynamics research trends can be highlighted, as discussed in the following.

While the groundwork of fundamental knowledge about passive mode locking was established about two decades ago [2–4], there is currently a renewed interest in the study of mode-locking dynamics. This interest is motivated by several key objectives that comprise the understanding of the transition from noise to the mode-locked state in self-starting mode-locked lasers [5], the minimization of fluctuations in the mode-locked single-pulse operation in view of the generation of high-quality frequency combs [6,7], the search for novel cavity designs that allow high-energy pulses to be produced out of single-fiber oscillators [8,9], and related improved mapping tools such as variational methods or master equations [8,10,11].

A common understanding is that mode locking appears as an abrupt transition from a noisy cw operation to a clean short-pulsed laser operation. However, there can be significant deviations from this scenario. The existence of dispersive waves that are radiated by the pulse as it travels through the discontinuities of the laser cavity medium can significantly alter the spectral and temporal pulsed features [12]. The observation of noiselike pulses is an example of puzzling dynamics that does not fall into the conventional picture of a mode-locked operation [13]. The intriguing recent finding of *soliton rain* dynamics corresponds to an intermediate regime where soliton pulses and cw components of comparable strength not only coexist but also interact in a dramatic way [14]. In soliton rains, new soliton pulses spontaneously form from a noisy background and drift at nearly constant velocity until they reach a condensed soliton phase, which is an aggregate of several tens of bound solitons.

Soliton rains, since they comprise several tens of pulses and their intracavity interactions, belong to the category of multiple-soliton dynamics. Multiple pulsing is frequently met in fiber lasers and is the typical result of the conjunction of a relatively strong pumping power of hundreds of milliwatts with propagation in an anomalously dispersive cavity. According to the laser cavity configuration and settings, it can take various forms [1]. The intracavity pulses can have erratic relative motions, stabilize themselves at more or less random relative positions, or distribute themselves regularly all along the cavity [15]. The latter situation, called harmonic mode locking, can be understood as resulting from a weak repulsive force attributed to the gain medium depletion and the recovery time between subsequent solitons [16]. Pulse bunching is another possible behavior that corresponds to the ability of several identical soliton pulses to group themselves in a stable and tight packet whose duration is much smaller than the cavity round-trip time [17,18]. Subclasses of pulse bunches have been investigated and reinterpreted as soliton molecules [1,19] in the framework of dissipative soliton dynamics, an important field of nonlinear science whose development in the past decade has been considerable [20]. A remarkable distinct feature of dissipative solitons is indeed their tendency to aggregate into stable bound states, or "soliton molecules" [21–25]. In the field of mode-locked laser dynamics, in addition to providing an explanation for stable soliton molecules, dissipative soliton concepts and models have been applied successfully in numerous situations to interpret unusual dynamics such as long-period soliton pulsations [26], soliton collisions [27], and vibrations of soliton pairs [28,29].

Dissipative soliton average models such as the cubic-quintic Ginzburg-Landau model provide a possible frame for understanding the coexistence of cw and dissipative soliton pulses that is at the heart of the soliton rain dynamics [30]. The existence of a cw component is also known to mediate interactions between solitons, thus strongly affecting multisoliton dynamics [31–33].

It is also very likely that additional physical ingredients, such as noise, will be required to explain the soliton rain

dynamics numerically. On the way toward building a comprehensive model able to reproduce soliton rains, it is therefore of great importance to perform a comprehensive experimental study, in the range of cavity settings where soliton rains manifest themselves, including a description of the surrounding dynamics. This is the aim of the present paper, which is organized as follows. Section II details the mode-locked fiber laser experimental setup and provides a gross description of the soliton rain dynamics as belonging to a set of weakly mode-locked dynamics. Section III provides a comprehensive experimental study of the soliton rain dynamics, when cavity parameters are altered, as well as when an external cw signal is injected inside the cavity. Descriptions of other remarkable dynamics that are manifest in the vicinity of soliton rains are gathered in Sec. IV. Section V provides discussions about key mechanisms involved in the interactions among the various field components of a soliton rain, and preliminary conclusions are given in the last section.

II. EXPERIMENTAL SETUP AND THE OBSERVATION OF SOLITON RAINS

Experiments are performed with the fiber laser setup sketched in Fig. 1. Passive mode locking is achieved through the ultrafast saturable absorber effect that results from the noninear polarization evolution taking place in the fibers, when it is followed by a polarization-dependent transmission [34]. The all-fiber ring laser cavity features dual 980-nm pumping of a 2-m-long erbium-doped fiber (EDF, normal dispersion $D = -12.5\ \mathrm{ps\,nm^{-1}\,km^{-1}}$), with a maximum injected power of 800 mW. The ring comprises in series a polarization-insensitive optical isolator that ensures unidirectional laser emission at $\lambda = 1.5\ \mu$m, a polarization controller made of small fiber loops (PC1), a 3% output coupler, a polarization splitter that provides the required polarization-dependent transmission for mode locking, a four-port 80:20 coupler that allows light injection, a second polarization controller (PC2), and a length of dispersion-compensating fiber ($D =$ $-91\ \mathrm{ps\,nm^{-1}\,km^{-1}}$). Except for a short length (0.15 m) of birefringent fiber at the output of the polarization splitter, fibered components are pigtailed with SMF-28. The overall cavity length is 13.5 m, yielding a round-trip time of 66 ns.

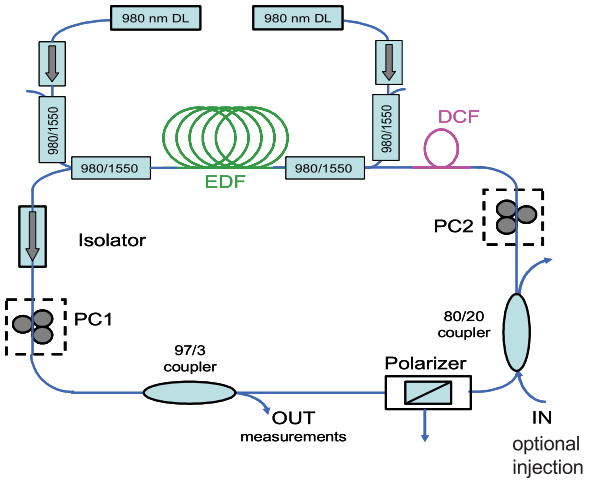

FIG. 1. (Color online) The all-fiber laser setup. EDF, erbium-doped fiber; DCF, dispersion compensation fiber; PC1,PC2, polarization controllers; 980/1550, wavelength multiplexer; DL, pumping diode laser.

The path-averaged dispersion can be changed stepwise by the inclusion of various lengths of the dispersion-compensating fiber (DCF). In the present study, unless otherwise specified, the cavity operates at an anomalous path-averaged chromatic dispersion ($\bar{D} = +5\ \mathrm{ps\,nm^{-1}\,km^{-1}}$). The orientations of the paddles of the polarization controllers, which can be recorded, define the shape of the intensity transfer function that in turn controls most of the pulsed dynamics [35]. In the first place, one has to find by trial and error the domains for the paddle orientations where stable mode locking can be found. Naturally, there is a pumping threshold in order to achieve mode locking, which is around 80 mW.

When we increase the pumping power, we observe the following trends. One expected trend is that the larger the pumping power, the wider the domains for paddle orientation that provide mode locking. In addition, increasing the pumping power readily provides multiple pulsing, which can manifest in a wide range of internal dynamics as discussed in the Introduction. When the total injected pumping power reaches its maximum of 800 mW, nearly 100 soliton pulses can coexist inside the cavity. One less expected trend that we observe is that the higher the pumping power, the wider—in terms of polarization-controller settings—the region where quasi-cw and soliton components can coexist. The existence of an extended transition between stable mode-locking dynamics and quasi-cw dynamics at high pumping power is illustrated in Fig. 2, which presents a succession of output optical spectra and temporal intensity recordings while the angle of one polarization controller (PC1) is varied. Optical spectra, plotted on a logarithmic scale, are recorded through an Anritsu MS9710B. Real-time recordings of the output field intensity are performed using a 6-GHz oscilloscope (Lecroy SDA6020), with a 5.6-GHz optical-electrical converter.

Figures 2(a) and 2(b) clearly show, from top to bottom, the gradual transition from a quasi-cw to a mode-locked dynamics. The injected pumping power is 600 mW. For the initial orientation of the polarizer controller, the laser operates with many longitudinal modes and arbitrary phase relationships between them, hence providing a noisy cw regime. Instead of providing a complete transition from cw to mode locking, the change of orientation of the PC produces first the appearance of a weak mode-locking component next to the cw components. as shown in Fig. 2(a) ($\theta = 90°$). As the PC is turned further, the mode-locked spectral components increase in intensity, while the cw components decrease until they practically disappear. Additional peaked spectral components appear at specific locations owing to dispersive wave radiation; these are phase-matched to soliton spectral components [12,32]. Radiated waves are indeed emitted by soliton pulses as they reshape during their travel through the inhomogeneities and discontinuities of the laser cavity. Corresponding to the gradual changes displayed in the spectral domain, Fig. 2(b) shows the output intensity oscilloscope traces which feature important modifications in the temporal domain. At large pumping power (600 mW), mode locking is readily associated with multiple pulsing. Rains of solitons are observed in the intermediate

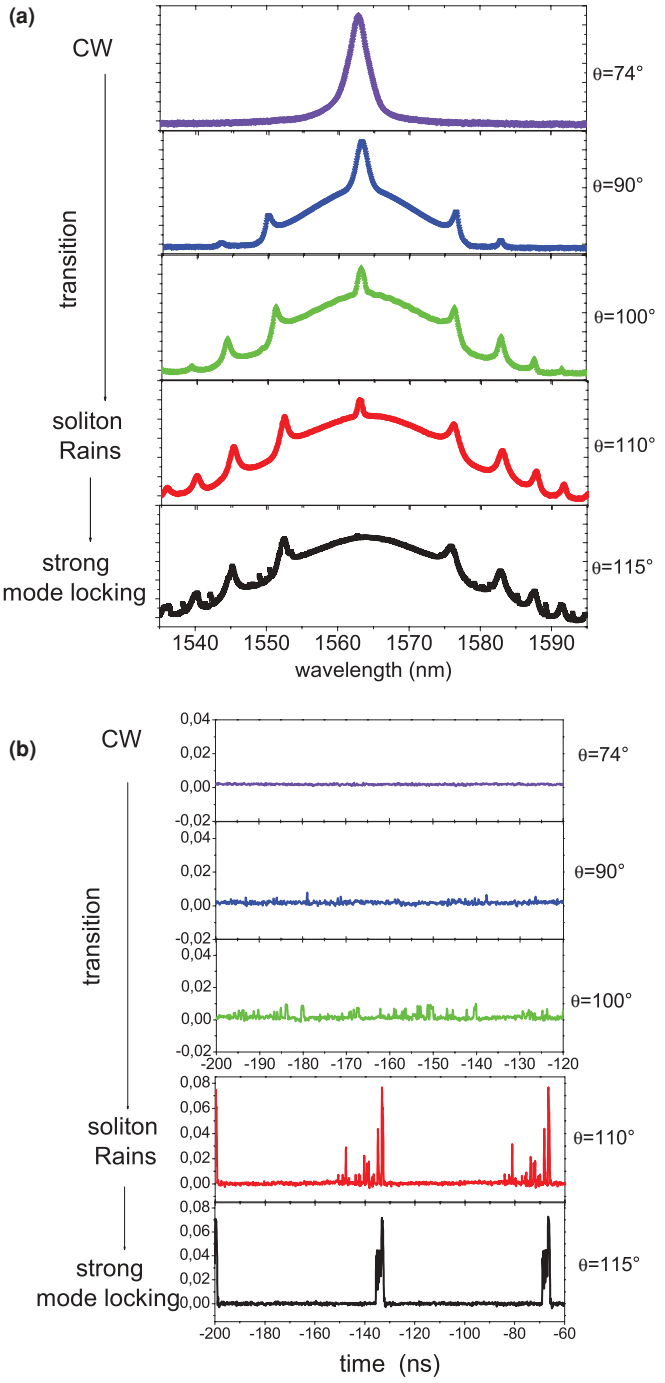

FIG. 2. (Color online) Progressive mode-locking transition obtained with the tuning of the first polarization controller (PC1). (a) From top to bottom, evolution of the optical spectra, in logarithmic scale, along with the PC orientation. (b) From top to bottom, corresponding evolution of oscilloscope recording of the output laser intensity, in linear scale.

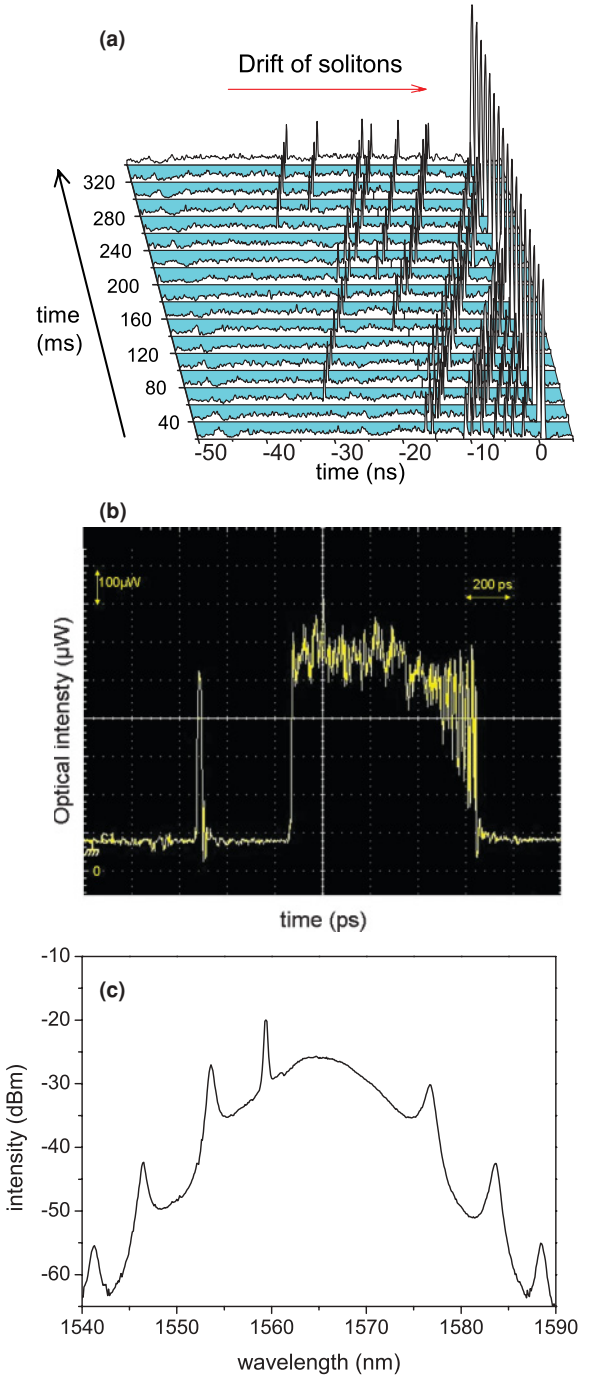

FIG. 3. (Color online) (a) Successive oscilloscope recordings of the output laser intensity showing stroboscopically the temporal dynamics of the soliton rain and its three field components: the noisy background, drifting solitons, and the condensed soliton phase which corresponds to the large peak on the right of each trace. (b) Temporal magnification of the condensed soliton phase, using a 30-GHz sampling scope. An incoming drifting soliton is also seen on the left. (c) Optical spectrum, showing soliton, cw, and radiation components.

regime where soliton pulses and cw components coexist and amount to comparable integrated energies [14]. We refer to this intermediate regime as one of *weak mode locking*, since low-intensity waves are not as efficiently filtered out as they are in the usual mode locking. A clear picture of the soliton rain dynamics is provided within Fig. 3(a), which consists of successive recordings of oscilloscope traces. Each trace monitors the real-time optical intensity, with subnanosecond resolution, at the laser cavity output.

Soliton rains consist of three field components: a noisy background, a set of isolated drifting solitons, and a condensed

soliton phase. The noisy background is produced by a large number of quasi-cw components. The origin of these quasi-cw components can be threefold: amplified spontaneous emission (ASE), cavity cw modes, and dispersive waves radiated from solitons. As mentioned above, dispersive waves produce almost symmetrically located spectral sidebands that are clearly visible on the optical spectrum. The major spectral component that is always present in the case of soliton rains, however, is distinct from these sidebands. It appears close to the maximum of the spectrum, on the short-wavelength side [Fig. 3(c)]. Since its width is rather small, around 0.5 nm, and it appears close to 1560 nm, it is not directly linked to ASE, but is reminiscent of the set of spectral components in the quasi-cw regime. Thus, the noisy background visible in Fig. 3 seems to be mostly based on a large number of cw cavity modes whose random beats produce significant fluctuations.

Above a certain threshold, these fluctuations can be readily amplified due to the conjunction of saturable absorption with a large gain per pass in the EDF. Pulse-shaping mechanisms, which take typically fewer than 100 cavity round trips in most numerical simulations of single-pulse mode locking [19], will experimentally provide popping out of the soliton pulse from the quasi-cw background on the microsecond time scale. Immediately after being created, the fixed-amplitude dissipative soliton will drift at a rather low speed that makes it observable in real time on the oscilloscope trace. The drifting time will be typically of the order of a second, at a nearly constant drifting speed, until the soliton reaches the condensed soliton phase that corresponds to the dominant peak on the oscilloscope traces. The drifting motion of solitons is well rendered in the stroboscopic picture of Fig. 3, and the quantization of the dissipative soliton energy is clearly manifested. The sign of the observed relative velocity between isolated drifting solitons and the condensed soliton phase is always the same: the condensed soliton phase moves faster than isolated drifting solitons. The location where isolated solitons are created from the background is not entirely random, since the average background level is not exactly constant. Between two successive passages of the condensed phase, the background level increases with time, and so does the probability of soliton creation. This variation of the background level can have several, possibly combined, origins: It might arise from the amplification in the EDF gain medium which is slightly relaxed after the passage of the condensed soliton phase, or result from an asymmetric radiation of the condensed soliton phase.

Since, on average, drifting solitons are created far apart (nanosecond separation) with respect to their temporal widths (around 1 ps), they will be considered as isolated from each other. This remains true only when the soliton rains does not exceed the order of ten created solitons per second. They will then drift at uniform speed. In the case of *heavy rains*, namely, when the probability per unit time of creation of several solitons at subnanosecond separation is increased by an order of magnitude, interactions and partial clustering can be observed. The rate of soliton creation will depend on cavity settings, as we shall see in the next section.

After drifting on top of the background, isolated solitons will collide with the condensed soliton phase. A temporal close-up view of the condensed phase is displayed in Fig. 3(b). This recording is obtained through a 30-GHz digitizing sampling oscilloscope, which does not provide real-time recording but an averaged temporal trace. Hence, it was not possible to observe the interaction between incoming drifting solitons and the condensed phase, although one incoming pulse was captured in the selected recording. However, this temporal recording contains several pieces of information. In addition to the precise measurement of the temporal spreading of the condensed phase, here 760 ps, some soliton substructure is clearly revealed. For that reason we used the terminology *condensed phase*. The multipeaked structure indicates the average location of soliton pulses inside the condensed phase. Solitons are not equally separated: the separation is reduced in the leading edge, where it falls below the temporal resolution level of around 20 ps. In addition, the positions of solitons are not well defined since there is a large timing jitter inside the condensed phase, which turns out to be somewhat analogous to a *liquid* phase. Finally, the number of solitons in the condensed phase can be calculated, either by direct soliton counting on the 30-GHz recording when it is possible, or from the ratio between the energy of the condensed phase and that of an isolated soliton, on real-time recordings. In the present case, there are around 40 solitons in the condensed phase. This typical number can also vary according to the cavity settings.

In terms of dynamics and energy flows, we get at this stage a rough picture of the interactions between the three field components of a soliton rain: the background, through the amplification of its random fluctuations, seeds the creation of drifting solitons, which in turn feed the condensed soliton phase. Since the size of the condensed phase remains constant on average, this means that the arrival of new solitons causes, possibly through collective rearrangements inside the condensed phase, the dissipation of a similar number of solitons. This dissipation could in turn produce additional radiation and dispersive waves that would contribute to the background.

Because of striking related analogies between the depicted dynamics and that of matter physics and the cycle of water in particular, we have called this dynamics a rain of solitons. Both types of dynamics operate in an open environment that contains a pump source providing a continuous supply of energy. The main limitation to the analogy lies in the fact that no conserved soliton quantities can be derived in a strongly dissipative nonlinear optical environment.

III. STUDY OF SOLITON RAIN DYNAMICS

We looked for, but did not find any soliton rain in the case of a normal averaged chromatic dispersion, using the available pumping power. We found soliton rain dynamics for $D = +5\ \mathrm{ps\,nm^{-1}\,km^{-1}}$ (with a 1 m length of DCF) as well as for $D = +10\ \mathrm{ps\,nm^{-1}\,km^{-1}}$ (without DCF). The soliton rain was more stable and existed within a larger domain of cavity settings with $D = +5\ \mathrm{ps\,nm^{-1}\,km^{-1}}$, so that, unless otherwise stated, the reported studies concern this value of the chromatic dispersion.

A. Influence of the polarization-controller settings

The use of a nonlinear polarization evolution to mode-lock the fiber laser provides many degrees of freedom to

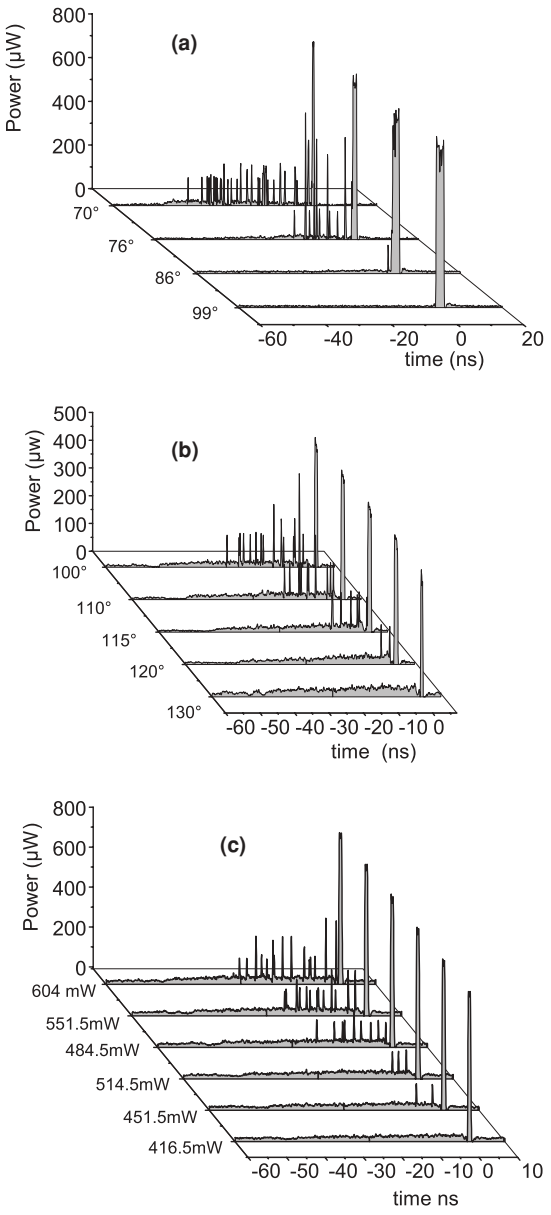

FIG. 4. Influence of cavity settings. (a) Reduction of background and stopping of soliton rain along with change in polarization-controller angle. (b) Alternative behavior where background increases while the soliton rain gradually ceases. (c) Increase of pumping power leading to soliton rain.

the effective nonlinear transfer function resulting after the polarizer, which can be accessed through simple turning of the polarization controllers [35]. The drawback is that it is a nontrivial problem to obtain the relationship between the particular set of angles of the PCs and the nonlinear transfer function [11,36]. However, the exploration of these degrees of freedom can be performed in a heuristic but reproducible way in the experiment. The use of at least two PCs is required to perform this exploration.

Two distinct trends that depend on the PCs are illustrated in Figs. 4(a) and 4(b). In Fig. 4(a), the modification of the PC angle from 70° to 99° produces a reduction of the background as well as stopping the soliton rain, on the way to a regime strongly dominated by mode locking with multiple aggregated pulses, as also presented in Fig. 2. There is another possible trend, displayed on Fig. 4(b), where the change of the PC's orientation (from 100° to 130°) produces an increase of the background but with a stopping of the soliton rain. The level of fluctuations required to form soliton pulses has increased more than the average background, and this can be understood as a shift of the effective saturable absorption to higher intensity values.

We have measured the relative speed of drifting solitons with respect to the condensed soliton phase that always serves as the triggering event. The speed is stable for a given cavity setting but depends on the setting of the PCs. Experimenting with the orientations of the PCs, we measured a drifting speed ranging from 3 to 27 $\mathrm{m\,s^{-1}}$.

B. Pumping power influence

When the PC settings favor the existence of soliton rains, there is obviously a pumping power threshold required to simultaneously fuel the existence of the three soliton rain components: the condensed soliton phase, the noisy cw background, and drifting solitons. This is illustrated in Fig. 4(c). First, mode locking coexists with the large cw background ($P = 416$ mW). When a certain pumping power threshold is reached, here $P = 430$ mW, the level of fluctuations in the cw background is increased above the level required for the formation of additional solitons, so that the soliton rain starts with one or two drifting solitons. Subsequent increase of the pumping power ($P = 484$–551 mW) increases the number of drifting solitons and eventually unleashes a heavy soliton rain ($P = 604$ mW). In the latter case, the probability that two solitons are created closer together than the temporal resolution of the oscilloscope becomes important; hence the presence of peaks of multiple amplitudes. Using stroboscopic recording, we also obtained indication of interactions between drifting solitons in the case of heavy soliton rains. A notable fact is that the level of pumping power did not influence the drifting speed of isolated solitons ($P = 430$–550 mW).

C. External control of soliton rain

In addition to using the pumping power threshold, there is another means to directly control the appearance or disappearance of the soliton rain. Since the soliton rain appears above a certain threshold of the noisy cw background that is fixed by the settings of the polarization controllers, it is possible to increase that cw level by injecting light into the cavity. A fine control of the amount of the injected light should initiate or stop the soliton rain.

We have demonstrated this possibility by injecting an external cw laser from the available input port of the 80:20 coupler [14]. The injected light is produced by a narrowband tunable laser (Photonetics PRI), and its intensity is adjusted by an attenuator. The pumping power is adjusted so that the laser dynamics is close to the soliton rain threshold, with the injected laser "off." Right after switching "on" the injected laser, the soliton rain starts and lasts as long as injection continues. When injection is turned of, the soliton rain stops almost immediately, right after the last soliton created finishes its drift to the condensed phase. The required injected switching power is as

small as 10 μW. However, the efficiency of the external control depends on the wavelength of the injected laser compared to the center of the spectrum of the soliton component. The injected laser can trigger soliton rain only when its wavelength is on the short-wavelength side of the soliton spectrum. For instance, with a soliton spectrum centered at 1560 nm, the wavelength of the cw laser could be chosen between 1545 and 1560 nm, with optimal efficiency around 1553 nm. In addition, the drifting speed of solitons could be varied according to the power level of the injected cw laser. While in the range 10–100 μW, no significant speed variation was observed; the drifting speed dropped from 12 to 5 m/s when the injected power level increased from 100 to 220 μW.

D. Soliton rain harmonics

Quite surprisingly, we also observed multiple soliton rain dynamics per cavity round trip, at high pumping power (600 mW) and for specific orientations of the PCs. Although harmonic mode locking is a common dynamical feature of mode-locked lasers operating under high pumping power, it was unexpected to observe cavity harmonics of complicated collective dynamics such as the soliton rain.

Figure 5 features oscilloscope recordings that show second cavity [Fig. 5(a)] and third cavity soliton rain harmonics [Fig. 5(b)]. Although very similar in terms of average number of drifting solitons, level of background, and size of the condensed phase, the two or three soliton rain harmonics that coexist in a cavity round trip are not exactly the same because of the randomness associated with the formation of solitons from each part of the background.

The existence of soliton rain harmonics can be partly explained by some instability of the condensed phase when its size exceeds a certain level that is typically around 40 solitons: the condensed phase breaks into parts, the energy is redistributed at symmetrical relative locations, and each new condensed phase becomes specifically related to a part of the background that produces drifting solitons.

IV. OTHER RELATED COLLECTIVE SOLITON DYNAMICS

The range of cavity settings that provide the soliton rain dynamics is rather large: the pumping power can be varied by typically more than 20%, the angle of the PCs can be changed by typically 5°–10°. We have explored the vicinity of the domain of existence of soliton rains to gain more insight into collective soliton behaviors that could be related to the soliton rain dynamics.

A. Chirped trains plus condensed soliton phase

In the chirped train dynamics that is illustrated by Fig. 6, individual solitons have ceased their drift motion with respect

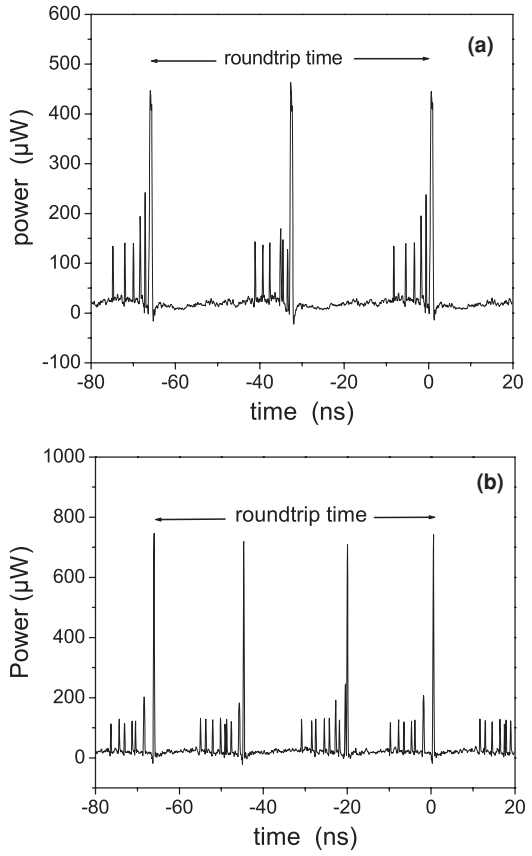

FIG. 5. Soliton rain harmonics: (a) second cavity soliton rain harmonic at 30 MHz repetition rate, twice the fundamental cavity repetition rate, and (b) third cavity soliton rain harmonic (at 45 MHz).

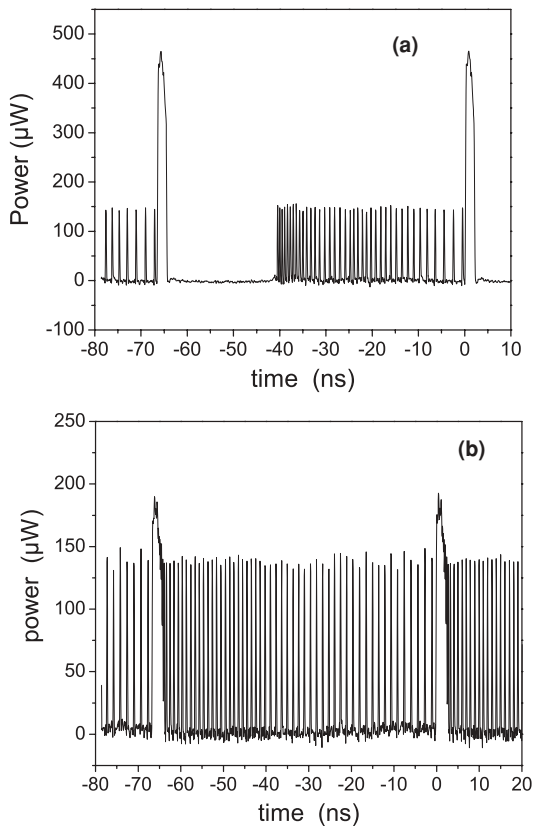

FIG. 6. Chirped soliton trains that are accompanied by condensed soliton phases: (a) chirped train partly filling the cavity and attached to a single condensed phase, and (b) chirped train filling the entire cavity.

to the condensed soliton phase that is still there. The individual (namely, temporally resolved) solitons organize with their neighbors in a train of pulses whose separation increases with time; hence the *chirped train* terminology.

In terms of cavity settings, this chirped soliton train dynamics is particularly close to the domain of existence of soliton rains and is obtained through a change of orientation of a PC that significantly reduces the amount of noisy cw background. However, a small background is still present and could play an important role in mediating interactions between solitons.

In Fig. 6(a), the chirped train occupies about two-thirds of the cavity round trip and is attached at the end to the condensed soliton phase. This extension of the chirped train can be almost continuously selected by a fine tuning of the orientation of the PC (within 1°, typically). The existence of chirped trains, where the temporal separation between adjacent pulses increases along the train, might be related to two mechanisms. On the first hand, gain relaxation dynamics entails that the leading pulses experience a little more gain than the trailing pulses, which feel the equivalent of a repulsive force. It seems plausible that gain relaxation dynamics, despite the long relaxation time of the erbium metastable state (10 ms), plays a significant role at the nanosecond time scale. On the other hand, the inhomogeneous distribution of background, part of which comes from soliton radiation, can play an important role in establishing a stationary binding distance between subsequent pulses. Indeed, the stronger the radiation, the greater the distance over which soliton pulses can bind through radiation-mediated interaction [32].

Figure 6(b) shows the situation when the chirped train fills the entire cavity and links to condensed phases at both ends. This latter situation is puzzling if one invokes the gain relaxation dynamics alone, since the gain depletion after the condensed phase, which comprises tens of closely aggregated solitons, should be large enough to increase significantly the separation between subsequent solitons. Thus, it is likely that the nonuniformity of the background becomes the dominant mechanism in establishing the nonuniformity of soliton-soliton spacing. Hence, the existence of a temporally asymmetric radiation from the condensed soliton phase is indicated as the main origin of chirped soliton trains.

B. Harmonic mode locking

Changing the cavity settings a little further from the soliton rain, having passed from the stationary chirped train dynamics, we now obtain the harmonically mode-locked regime. In the most favorable case, it corresponds to equally separated solitons, hence providing a significantly increased output repetition rate. This case is illustrated by Fig. 7, which shows the 82nd cavity harmonic with a repetition rate of 1.24 GHz. High-order cavity harmonics in fiber lasers have been investigated for more than a decade, and the initial conclusion was that the output repetition rate is difficult to stabilize in general [15,37], so that researchers subsequently developed active or passive-active harmonic mode-locking strategies [38]. We here confirm the difficulty of selecting the cavity settings and precise orientations of PCs that yield stable high-harmonic output with good supermodal suppression, as displayed on Fig. 7(b).

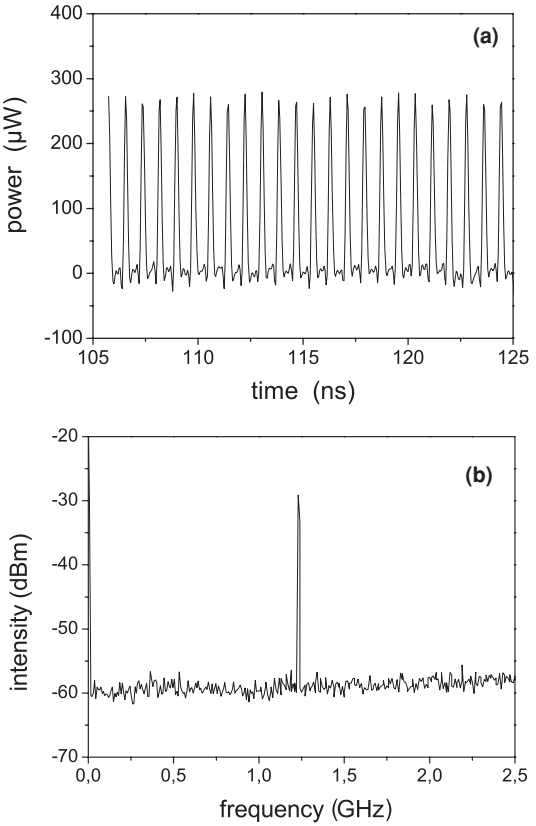

FIG. 7. 82nd-harmonic mode locking: (a) optical intensity and (b) corresponding radio-frequency spectrum.

Among other possible mechanisms, the equalization of interpulse separation through depletion and recovery of the gain medium has often been suggested in harmonic passively mode-locked lasers [16], and seems plausible in our present situation. However, the influence of a cw background cannot be ruled out, since cw peaks remained in the optical spectrum; however, the whole background appeared distributed uniformly in the temporal domain.

C. Release of solitons from the condensed phase

As we try to understand the soliton rain dynamics, the following question arises naturally: What determines the relative motion of the drifting solitons with respect to the condensed phase?

The optical spectrum recorded for a soliton rain features asymmetry that should be related to the temporal asymmetry of the dynamics, in the presence of chromatic dispersion. A typical soliton rain spectrum is presented in Fig. 8(a): it always features a cw peak on the short-wavelength side close to the center of the soliton spectrum, as well as stronger soliton sidebands on the short-wavelength side. This preferred asymmetry can be attributed to the existence of a stronger gain of the erbium medium on the short-wavelength side—the gain peaks at around 1535 nm.

However, we found specific settings of the PCs that produced an inversion with respect to the dominant spectral

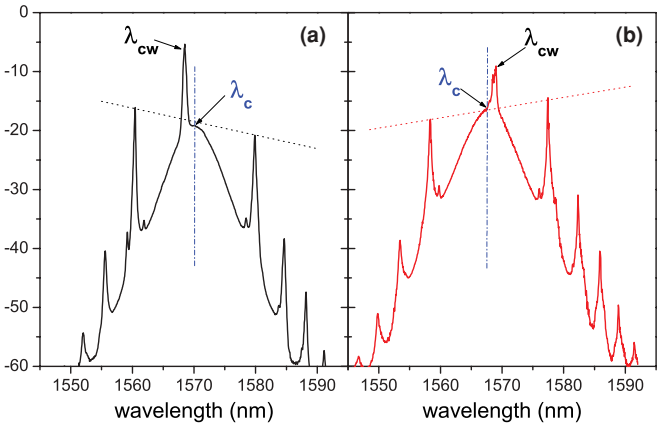

FIG. 8. (Color online) Comparison between optical spectra typical in the case of (a) soliton rains, where individual solitons flow toward the condensed phase, and (b) quasistationary release of solitons from the condensed phase.

asymmetry, as shown in Fig. 8(b). Both the cw and soliton sideband components now dominate on the long-wavelength side of the soliton spectrum. Then we observed a major difference in the temporal dynamics: Instead of drifting toward the condensed phase, the solitons were coming out of it, flowing outward until they vanished in the background. Using again a stroboscopic recording of the output intensity, this dynamics is presented in Fig. 9. At this stage, it becomes clear that the precise composition of the spectrum and the impact of chromatic dispersion dictate the temporal dynamics, as discussed in the next section.

V. DISCUSSION

Dissipative solitons and quasi-cw background can coexist in an erbium-doped fiber laser. We observed that the stronger the pumping power, the larger this region of coexistence. It can be understood in the framework of high-order nonlinear

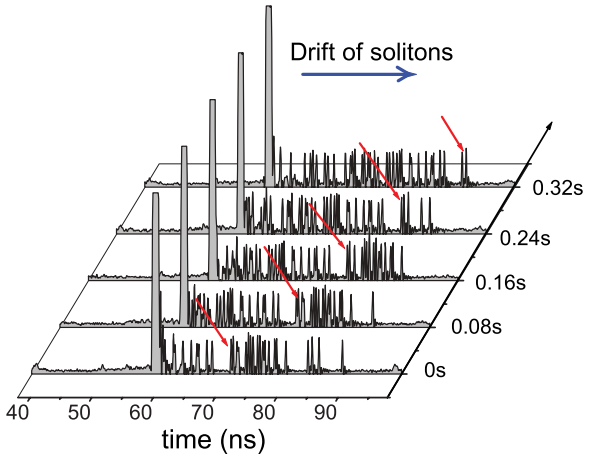

FIG. 9. (Color online) Stroboscopic recording of the quasistationary release of solitons from the condensed soliton phase. This temporal dynamics is associated with the optical spectrum of Fig. 8(b).

propagation models, such as the cubic-quintic Ginzburg-Landau equation: Cubic-quintic equations allow for the coexistence of several cw and soliton solutions, although some of them can be unstable [30]. In addition, the set of intensity transfer functions that can be obtained through nonlinear polarization-evolution mode locking, when the settings of the polarization controllers are varied, is particularly large, providing favorable experimental conditions for the discovery of unusual dynamics.

Use of strong pumping power in an anomalous path-averaged dispersion laser also yields a large number of solitons, typically of the order of 50 in our experiment. Some of these solitons are likely to interact, for instance leading to the formation of a condensed soliton phase, with a binding range between solitons of the order of 10–20 ps, that is, a separation compatible with previous observations of soliton molecules in mode-locked fiber lasers [19]. However, solitons do not stay at rest in the moving frame of the condensed phase; their positions are fluctuating with time as if they were in a liquid thermodynamical phase. These important position fluctuations can be attributed to the large amount of noisy radiation on top of which solitons exist.

The noisy cw background is composed of two main contributions. One contribution comes from soliton sidebands that are typical of mode-locked fiber lasers operating in the anomalous dispersion regime. In the case of a second-order dispersion dominant over third-order chromatic dispersion, these sidebands are symmetrically located with respect to the center of the soliton spectrum (indicated as λ_c on Fig. 8). In the case of a highly pumped fiber laser, the first pair of symmetrical soliton sidebands is clearly of significant magnitude: We can see in Fig. 8, around each dominant soliton spectral sideband, the presence of tiny spectral sidebands that arise from the modulational instability of these quasi-cw waves. The other contribution to the overall noisy cw background comes from the set of cw modes that coexist with solitons (λ_{cw} on Fig. 8). The spectral width of the latter peak, being around 0.5 nm, contains a large number of longitudinal modes whose random beats produce the fluctuations required to create additional soliton pulses.

In the case of soliton rain dynamics, the soliton part of the spectrum is centered at a longer wavelength than the wavelength of the dominant cw components [Fig. 8(a)]. In anomalous dispersion, this results in radiation traveling faster than solitons. This explains why radiation from the condensed phase is more pronounced on the leading edge side (left part of the oscilloscope trace), and why solitons can move to the right relative to it. Although we do not fully understand the relative motion between isolated solitons and the condensed soliton phase, there could be several reasons for this: A bound state of solitons generally corresponds to a different spectrum than that of isolated solitons; hence there is a possible relative motion caused by chromatic dispersion or spectral filtering effects [1,27]. Also, the strong interaction between solitons and the background inside the condensed phase could alter their group velocity.

The radiation of the condensed soliton phase is an important part of the whole soliton rain dynamics. Assuming a quasistationary dynamics—indeed, the soliton rain dynamics is not a transient event, but can last for hours when the fiber laser

settings are not altered—the noisy cw background transfers energy to newly created solitons, and then these drifting solitons transfer energy to the condensed soliton phase. In order for the latter not to grow indefinitely, it should radiate significantly. Hence our present understanding of soliton rains is based on dissipative nonlinear dynamics among these three interacting field components.

VI. CONCLUSION

The recently discovered soliton rain dynamics is a complex but beautiful illustration of self-organization among large numbers of solitons and radiation. Observed in a fiber laser that is operated in the highly pumped but weakly mode-locked regime, when both soliton pulses and cw background coexist, soliton rains are obviously a manifestation of dissipative nonlinear dynamics. It is characterized by the interactions among three main field components. The first component is a bunch of several tens of bound jittering solitons which we have called the condensed soliton phase, since it seems analogous to a liquid thermodynamical phase. Just as a liquid would evaporate, the condensed phase emits a large amount of radiation on one temporal side. That radiation indeed moves to shorter times owing to the conjunction of anomalous dispersion and spectral asymmetry of the radiated waves. This radiation is also superimposed on other preexisting cw modes, and they altogether produce a noisy, inhomogeneous background with large fluctuations. When fluctuations exceed a certain level, a new soliton is formed, like a droplet formed from a vapor cloud, and then drifts back to the condensed phase at a nearly constant relative velocity. The whole scenario repeats in a quasistationary fashion.

In addition to interesting analogies with the cycle of water, the soliton rain dynamics addresses the largely unexplored field of nonlinear dissipative dynamics in the case of large soliton numbers, brings useful information in the context of mode-locking dynamics, and illustrates the diversity of operating regimes accessible in fiber lasers mode-locked through nonlinear polarization evolution. In practice, we have shown the influence of cavity settings on soliton rain dynamics, which can be used for external control of the dynamics as well, and presented neighboring dynamics that help in understanding the soliton rain. In spite of the complexity of the dynamics, the present experimental study paves the way for the building of a comprehensive theoretical model of soliton rains.

ACKNOWLEDGMENTS

S.C. acknowledges financial support from Conseil Régional de Bourgogne and from Université de Bourgogne.

[1] Ph. Grelu and J. M. Soto-Crespo, in *Dissipative Solitons: From Optics to Biology and Medicine*, Vol. 751 of *Lecture Notes in Physics*, edited by N. Akhmediev and A. Ankiewicz (Springer-Verlag, Berlin, 2008), pp. 137–173.
[2] H. A. Haus, J. Appl. Phys. **46**, 3049 (1975).
[3] F. Krausz, T. Brabec, and Ch. Spielmann, Opt. Lett. **16**, 235 (1991).
[4] H. A. Haus, E. P. Ippen, and K. Tamura, IEEE J. Quantum Electron. **30**, 200 (1994).
[5] A. Gordon and B. Fischer, Phys. Rev. Lett. **89**, 103901 (2002).
[6] O. Basis and O. Gat, Phys. Rev. E **79**, 031126 (2009).
[7] J. K. Wahlstrand, J. T. Willits, T. R. Schibli, C. R. Menyuk, and S. T. Cundiff, Opt. Lett. **32**, 3426 (2007).
[8] N. Akhmediev, J. M. Soto-Crespo, and Ph. Grelu, Phys. Lett. A **372**, 3124 (2008).
[9] W. H. Renninger, A. Chong, and F. W. Wise, Opt. Lett. **33**, 3025 (2008).
[10] B. G. Bale and J. N. Kutz, J. Opt. Soc. Am. B **25**, 1193 (2008).
[11] A. Komarov, H. Leblond, and F. Sanchez, Phys. Rev. E **72**, 025604(R) (2005).
[12] J. P. Gordon, J. Opt. Soc. Am. B **9**, 91 (1992).
[13] M. Horowitz, Y. Barad, and Y. Silberberg, Opt. Lett. **22**, 799 (1997).
[14] S. Chouli and Ph. Grelu, Opt. Express **17**, 11776 (2009).
[15] A. B. Grudinin and S. Gray, J. Opt. Soc. Am. B **14**, 144 (1997).
[16] J. N. Kutz, B. C. Collings, K. Bergman, and W. H. Knox, IEEE J. Quantum Electron. **34**, 1749 (1998).
[17] M. J Guy, D. U. Noske, and J. R. Taylor, Opt. Lett. **18**, 1447 (1993).
[18] F. Gutty, Ph. Grelu, N. Huot, G. Vienne, and G. Millot, IEEE Electron. Lett. **37**, 745 (2001).
[19] Ph. Grelu, F. Belhache, F. Gutty, and J. M. Soto-Crespo, J. Opt. Soc. Am. B **20**, 863 (2003).
[20] *Dissipative Solitons*, Vol. 661 of *Springer Lecture Notes in Physics*, edited by N. N. Akhmediev and A. Ankiewicz (Springer-Verlag, Berlin, 2005).
[21] N. Akhmediev, A. Ankiewicz, and J. M. Soto-Crespo, Phys. Rev. Lett. **79**, 4047 (1997).
[22] Ph. Grelu and J. M. Soto-Crespo, Opt. Lett. **27**, 966 (2002).
[23] Ph. Grelu, F. Belhache, F. Gutty, and J. M. Soto-Crespo, J. Opt. B: Quantum Semiclass. Opt. **6**, S271 (2004).
[24] A. Zavyalov, R. Iliew, O. Egorov, and F. Lederer, Phys. Rev. A **80**, 043829 (2009).
[25] F. Amrani, A. Haboucha, M. Salhi, H. Leblond, A. Komarov, and F. Sanchez, Appl. Phys. B **99**, 107 (2010).
[26] J. M. Soto-Crespo, M. Grapinet, Ph. Grelu, and N. Akhmediev, Phys. Rev. E **70**, 066612 (2004).
[27] Ph. Grelu and N. Akhmediev, Opt. Express **12**, 3184 (2004).
[28] M. Grapinet and Ph. Grelu, Opt. Lett. **31**, 2115 (2006).
[29] J. M. Soto-Crespo, Ph. Grelu, N. Akhmediev, and N. Devine, Phys. Rev. E **75**, 016613 (2007).
[30] J. M. Soto-Crespo, N. Akhmediev, and G. Town, J. Opt. Soc. Am. B **19**, 234 (2002).
[31] S. Wabnitz, J. Opt. Soc. Am. B **13**, 2739 (1996).
[32] J. M. Soto-Crespo, N. Akhmediev, Ph. Grelu, and F. Belhache, Opt. Lett. **28**, 1757 (2003).

[33] D. Y. Tang, L. M. Zhao, B. Zhao, and A. Q. Liu, Phys. Rev. A **72**, 043816 (2005).
[34] V. Matsas, T. Newson, D. Richardson, and D. Payne, Electron. Lett. **28**, 1391 (1991).
[35] G. Martel, C. Chédot, A. Hideur, and Ph. Grelu, Fiber Integr. Opt. **27**, 320 (2008).
[36] E. Ding and J. N. Kutz, J. Opt. Soc. Am. B **26**, 2290 (2009).
[37] F. Amrani, A. Haboucha, M. Salhi, H. Leblond, A. Komarov, Ph. Grelu, and F. Sanchez, Opt. Lett. **34**, 2120 (2009).
[38] M. Horowitz, C. Menyuk, T. Carruthers, and I. Duling, J. Lightwave Technol. **18**, 1565 (2000).